Wei *et al.*
*EURASIP Journal on Advances in Signal Processing* (2022) 2022:125
https://doi.org/10.1186/s13634-022-00964-2

EURASIP Journal on Advances in Signal Processing

RESEARCH Open Access

# Performance analysis on the speed spectrum estimation based on dual-HFM waveform

Runyu Wei[1], Xuan Li[1,2*], Yubin Fu[1,2] and Xiaochuan Ma[1,2]

*Correspondence: lixuan@mail.ioa.ac.cn

[1] Laboratory of Autonomous Underwater Vehicles, the Institute of Acoustics, Chinese Academy of Sciences, Beijing, China
[2] University of Chinese Academy of Sciences, Beijing, China

**Abstract**

Real-time Doppler estimation of sonar signals is of great significance to underwater communication and detection. The Hyperbolic-Frequency-Modulated (HFM) waveform-based speed spectrum estimation is one of the modern methods for underwater Doppler estimation, and this paper presents a detailed analyses of the derivation and the performance of this method. The analyzing results show the robustness of the method on multipath channels and multi-highlight targets and provide the main lobe width of the speed spectrum. Moreover, the paper examines the spectral properties of the HFM signal from the frequency-domain Doppler invariance property, which could provide insights for better understanding and utilization of this Doppler invariant waveform.

**Keywords:** Doppler estimation, Underwater communication, HFM

## 1 Introduction

The Doppler scale estimation of sonar signals plays a critical role in underwater communication and detection systems. The method of matching the received signal with different Doppler copies of the transmitted signal is a universal solution, and its performance depends on the ambiguity function of the transmitted waveform. However, it requires a large amount of calculation to obtain a high-precision estimate [1]. The block Doppler estimation method inserts two synchronous waveforms before and after the signal segment, respectively, to obtain the average Doppler parameter [2]. This method is efficient for estimating the average speed but leads to a downgraded real-time performance.

The combination of two HFM signals with different sweeping directions provides a modern Doppler estimation solution in the past decade. Due to the excellent Doppler tolerance of the HFM signal, the combined HFM waveform is introduced into the preamble of underwater acoustic communication. This waveform is also called the UMD-HFM [3] or dual-HFM [4] signal. The classic methods include the double delay difference method [5, 6] and the correlation peak matching (CPM) method [7], and experimental results have confirmed the effectiveness of this waveform in Doppler estimation tasks.

Based on the spectrum properties of the HFM waveform, a speed spectrum scanning method was proposed for Doppler estimation [4]. This method makes full use of the Doppler invariance of the HFM signal in the frequency domain and produces

continuous high-accuracy speed estimates. However, theoretical analysis of the performance of this method has not been mentioned, despite its success in field experiments. In practical applications, the underwater acoustic (UWA) channel produces a multipath propagation phenomenon, and the echo of the target to the active incident sonar signal usually appears as multiple or distributed highlights. Therefore, in this paper, we specifically analyzed the effectiveness of the dual-HFM speed spectrum method in the multipath UWA channel, as well as the relation between the main lobe width of the speed spectrum and the transmitted waveform parameters.

Before giving out the speed spectrum method, it is necessary to analyze the spectral properties of the HFM waveform in detail. This waveform, which is very similar to bats, dolphins and other biological sonar signals, has excellent Doppler tolerance and has been widely used in sonar systems. Previous studies mainly focus on its time-domain properties. Although there have been approximate expressions for its spectrum, they are derived from the time-domain waveform and the stationary phase approximation. In this paper, the spectral properties of the HFM waveform are derived in terms of the ideal Doppler invariant (DI) signal, and the result is consistent with that of the stationary phase approximation. An understanding of the frequency-domain Doppler invariance of the HFM signal will help better utilize this waveform.

The paper is organized as follows. Section 2.1 introduces the HFM waveform and its time-domain Doppler invariance property. Section 2.2 analyzes the spectral properties of the ideal Doppler invariant (DI) signal and presents their relations with the HFM signal. Section 3.1 introduces the speed spectrum estimation method and gives the resolution performance analysis based on the spectral properties of the HFM waveform. Section 3.2 discusses the robustness of the proposed method on the UWA multipath channel and the multi-highlight targets. Section 4 gives out results and discussions of the speed spectrum. Section 5 makes a conclusion.

## 2 HFM properties

### 2.1 HFM waveform and the Doppler invariance

The Doppler effect occurs when the sound source or the receiver is moving, and the received signal appears to be the time-domain expansion of the source waveform. Let $s(t)$ be the source signal and $x(t)$ be the received signal, then

$$x(t) = A \cdot s(k(t-\tau)) \tag{1}$$

where $A$ is the amplitude, $\tau$ is the propagation time, and $k$ is the Doppler scaling factor. The Doppler scaling factor is closely related to the speed of the source or the target, e.g., $k = c/(c+v)$ in the scene of underwater communication with a moving source, where $c$ is the speed of sound and $v$ is the moving away speed of the source. This effect is significant for both underwater communication and active detection or positioning, because the received signal cannot accurately match the transmitted waveform, which leads to an increase in code error rate in communication, or the degradation in performance of target detection and parameter estimation. The accurate estimation of the Doppler information will massively alleviate the negative effect, and the estimate of the speed of the source or the target is usually valuable.

The Doppler invariant signal refers to the waveform that can be closely matched with its Doppler scaled copy. And the HFM waveform is one of those Doppler tolerant signals. The HFM signal waveform with frequency sweeping range $(f_l, f_h)$ and duration $T$ is expressed as

$$s_{\mathrm{HFM}}(f_l, f_h, T, t) = \exp\left[-j2\pi \frac{f_0^2}{M} \ln\left(1 - \frac{M}{f_0}t\right)\right] \tag{2}$$

where $-T/2 < t < T/2$, $j = \sqrt{-1}$, $f_0 = 2f_l f_h/(f_l + f_h)$ is the instantaneous frequency at $t = 0$, and $M = 4f_l f_h(f_h - f_l)/\left((f_l + f_h)^2 \cdot T\right)$ is the frequency modulating factor. We will hereinafter omit $f_l$ and $f_h$ for they are invariable. The instantaneous frequency of the HFM signal $f_t(T, t) = f_0(1 - Mt/f_0)^{-1}$ is a hyperbolic function. By taking the derivative, we have $\mathrm{dt}/\mathrm{df_t(T, t)} = \mathrm{M f_0^{-2}} \cdot [\mathrm{f_t(T, t)}]^{-2}$, which suggests the duration of the HFM waveform on frequency $f$ is proportional to $f^{-2}$, and the duration on the lower frequency is longer.

We temporarily omit the amplitude and the delay in (1), and then, the HFM signal with Doppler effect can be written as

$$s_{\mathrm{HFM}}(kt) = s_{\mathrm{HFM}}(t - \varepsilon(k)) \cdot \exp\left(j\vartheta(k)\right) \tag{3}$$

where $\varepsilon(k) = \frac{f_0}{M}\left(\frac{1}{k} - 1\right)$ and $\vartheta(k) = -2\pi \frac{f_0^2}{M} \ln k$. The approximation error comes from the difference between the definitional domains of $s_{\mathrm{HFM}}(kt)$ and $s_{\mathrm{HFM}}(t - \varepsilon(k))$, which is very small in the case of an infinitesimal $|v|/c$ and a large bandwidth. Therefore, the Doppler scaled HFM signal is almost a time-shift of the original waveform, which makes it closely matched with the transmitted waveform. This is the so-called Doppler invariance [8].

The spectrum of $s_{\mathrm{HFM}}(t)$ can only be accurately expressed with the incomplete gamma functions [9], but the approximate result can be obtained within the frequency range $(f_l, f_h)$ using the principle of stationary phase (PSP) [10].

$$S_{\mathrm{HFM}}(f) = \frac{f_0}{f\sqrt{M}} \cdot \exp\left(j\left(2\pi \frac{f_0}{M}\left(f_0 \ln f - f - \left(f_0 \ln f_0 - f_0\right)\right) + \frac{\pi}{4}\right)\right) \tag{4}$$

This method regards the phase term in the HFM signals as linear chirps and derives the spectrum using the approximation of the Fresnel integral. The approximation result is reasonable, but the derivation does not reveal the relationship between the spectral property and the Doppler invariance property of the HFM signal. In the next section, we will re-analyze this spectrum from the perspective of the Doppler invariance property.

### 2.2 Doppler invariant spectrum

We now put aside the waveform of the HFM signal and consider an ideal Doppler invariant (DI) signal $s_{\mathrm{DI}}(t)$ with an unknown waveform. The DI signal strictly satisfies the Doppler invariance

$$s_{\mathrm{DI}}(kt) = s_{\mathrm{DI}}(t - \varepsilon(k)) \cdot \exp\left(j\vartheta(k)\right) \tag{5}$$

where $\varepsilon(k)$ and $\vartheta(k)$ are derivable functions and $\varepsilon(1) = \vartheta(1) = 0$. This means that $s_{\mathrm{DI}}(t)$ has the same waveform as its Doppler scaled copy. Taking Fourier Transform on (5), then the spectrum of $s_{\mathrm{DI}}(t)$ satisfies the "frequency-domain Doppler invariance"

$$\frac{1}{k}S_{\mathrm{DI}}\left(\frac{f}{k}\right) = S_{\mathrm{DI}}(f) \cdot \exp\left[-j\left(2\pi f\varepsilon(k) - \vartheta(k)\right)\right] \tag{6}$$

Taking the modulus and the phase of (6) yields

$$\frac{1}{k}\left|S_{\mathrm{DI}}\left(\frac{f}{k}\right)\right| = \left|S_{\mathrm{DI}}(f)\right| \tag{7}$$

$$\Phi_{\mathrm{DI}}\left(\frac{f}{k}\right) = \Phi_{\mathrm{DI}}(f) - \left(2\pi f\varepsilon(k) - \vartheta(k)\right) \tag{8}$$

where $S_{\mathrm{DI}}(f) = \left|S_{\mathrm{DI}}(f)\right| \cdot \exp\left(j\Phi_{\mathrm{DI}}(f)\right)$. Substituting $k = \frac{1}{1+p}$ into (7) and making use of the derivative $\frac{\mathrm{d}|S_{\mathrm{DI}}(f)|}{\mathrm{d}f} = \lim_{p\to 0}\frac{|S_{\mathrm{DI}}[(1+p)f]|-|S_{\mathrm{DI}}(f)|}{pf}$ yields $\frac{\mathrm{d}|S_{\mathrm{DI}}(f)|}{\mathrm{d}f} = -\frac{|S_{\mathrm{DI}}(f)|}{f}$. Therefore, we obtain

$$\left|S_{\mathrm{DI}}(f)\right| = C \cdot \frac{1}{f} \tag{9}$$

which indicates that the signal satisfies the Doppler invariance must have an amplitude spectrum inversely proportional to $f$. Substituting $k = \frac{1}{1+p}$ into (8) and making use of the derivative $\frac{\mathrm{d}\Phi_{\mathrm{DI}}(f)}{\mathrm{d}f} = \lim_{p\to 0}\frac{\Phi_{\mathrm{DI}}[(1+p)f]-\Phi_{\mathrm{DI}}(f)}{pf}$ yields $\frac{\mathrm{d}\Phi_{\mathrm{DI}}(f)}{\mathrm{d}f} = \frac{2\pi f\varepsilon'(1)-\vartheta'(1)}{f}$, where $\varepsilon'(1)$ and $\vartheta'(1)$ are the derivatives of $\varepsilon(k)$ and $\vartheta(k)$ at $k = 1$, respectively. Through transposition and integration, we obtain

$$\Phi_{\mathrm{DI}}(f) = 2\pi f\varepsilon'(1) - \vartheta'(1)\ln f + \varphi_0 \tag{10}$$

where $\varphi_0$ is an arbitrary phase constant. So far, we have the frequency spectrum of the ideal DI signal $s_{\mathrm{DI}}(t)$

$$S_{\mathrm{DI}}(f) = \frac{C}{f} \cdot \exp\left[j\left(2\pi f\varepsilon'(1) - \vartheta'(1)\ln f + \varphi_0\right)\right] \tag{11}$$

where $C \cdot \exp\left(j\varphi_0\right)$ is a constant term and does not affect the waveform of $s_{\mathrm{DI}}(t)$. Meanwhile, $\varepsilon'(1)$ and $\vartheta'(1)$ completely determine the waveform and the spectrum of the DI signal. Since this spectrum expression is derived from the frequency-domain Doppler invariance (6), we call it "Doppler invariant spectrum." Taking the Fourier inverse transform generates the waveform of $s_{\mathrm{DI}}(t)$ as shown in Fig. 1. This is an infinitely long frequency sweeping signal with a hyperbolic instantaneous frequency. Because of the equivalence of time-domain energy and frequency-domain energy, the duration of $s_{\mathrm{DI}}(t)$ at frequency $f$ is proportional to $f^{-2}$ as $\left|S_{\mathrm{DI}}(f)\right|^2 \propto f^{-2}$.

It is not surprising that $s_{\mathrm{DI}}(t)$ is indeed an HFM signal with lower frequency $f_l = 0$ and upper frequency $f_h = \infty$. This infinitely long signal perfectly satisfies the Doppler invariance (5), and (2) is indeed a truncation of $s_{\mathrm{DI}}(t)$. The truncation produces an HFM

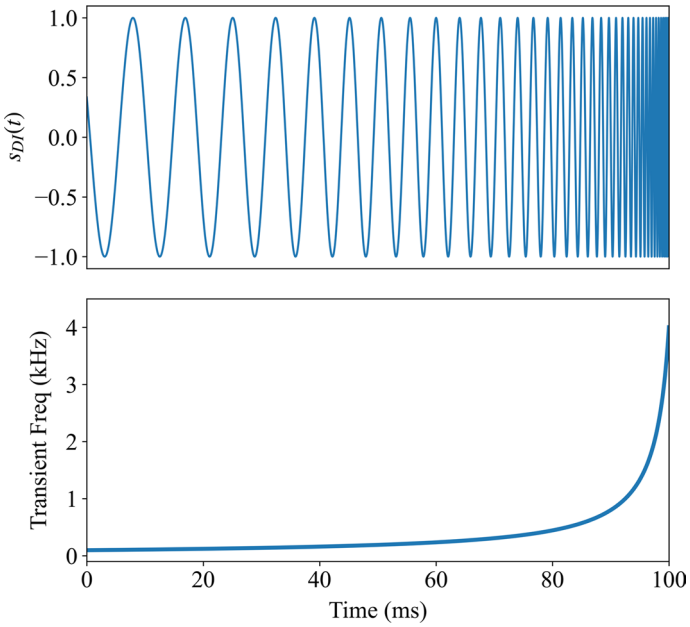


**Fig. 1** The waveform and instantaneous frequency of the ideal Doppler invariant signal $s_{\mathrm{DI}}(t)$

waveform with the band $(f_l, f_h)$, and its frequency spectrum is approximately the $(f_l, f_h)$ range of $S_{\mathrm{DI}}(f)$, despite a tiny difference (like a convolution with a sampling function). By substituting $\varepsilon(k)$ and $\vartheta(k)$ from (3) into (11), we can find that $S_{\mathrm{DI}}(f)$ is equivalent to the spectrum of the HFM signal, which means the HFM spectrum yielded by PSP is indeed the spectrum of $s_{\mathrm{DI}}(t)$. It further indicates that $s_{\mathrm{HFM}}(t)$ is exactly (a period of) $s_{\mathrm{DI}}(t)$ and the $S_{\mathrm{DI}}(f)$ derived from frequency-domain Doppler invariance is $S_{\mathrm{HFM}}(f)$, in which parameter $\varepsilon'(1)$ and $\vartheta'(1)$ depends on the frequency range and the pulse width. This derivation could help better understand and utilize the spectrum of this Doppler invariant waveform. It is worth pointing out that the derivation assumes the derivability of $S_{\mathrm{DI}}(f)$. Strictly speaking, it is possible for $s_{\mathrm{DI}}(t)$ to also be a constant signal otherwise.

Finally, we derive the spectral property of the differential HFM signal to prepare for the next section. Rewrite the spectrum of the HFM signal $s_{\mathrm{HFM}}(T,t)$ as $S(T,f) = \frac{C(T)}{f} \cdot \exp\left(j \cdot 2\pi \frac{f_0}{M}\left(f_0 \ln f - f + \varphi(T)\right)\right)$, where $C(T) = \frac{f_0}{\sqrt{M}}$ and $\varphi(T) = -f_0 \ln f_0 + f_0 + \frac{M}{8f_0}$ are the parameters independent of frequency. We will omit the subscript of $S_{\mathrm{HFM}}(f)$ in the following text. For any $\beta > 0$, we have

$$\mathcal{F}^{-1}\left[\left(f \cdot S(T,f)\right)^{\beta}\right] = \frac{(C(T))^{\beta-1}}{j2\pi\sqrt{\beta}} \exp\left(j \cdot \eta(T,\beta)\right) \cdot \frac{\mathrm{d}}{\mathrm{d}t} s_{\mathrm{HFM}}(\beta T, t) \tag{12}$$

for the HFM signal $s_{\mathrm{HFM}}(\beta T, t)$ with pulse width $\beta T$, where $\eta(T,\beta) = 2\pi \frac{\beta f_0}{M}(\varphi(T) - \varphi(\beta T))$ is independent of $t$. The differential HFM signal on the right side of the equation

$$\frac{\mathrm{d}}{\mathrm{d}t} s_{\mathrm{HFM}}(T,t) = j2\pi f_t(T,t) \cdot s_{\mathrm{HFM}}(T,t) \tag{13}$$

is still a frequency-modulated signal, but the amplitude is slowly changing.

## 3 Proposed method

### 3.1 Speed spectrum estimation

In the previous study, Wei [4] introduced the method of the speed spectrum estimation with dual-HFM waveform; therefore, this paper will omit most of the derivations and instead focus on the analysis of the estimation performance, which has not been investigated in the previous literature. Let the transmitted signal of the communication sonar or the active sonar system be the dual-HFM signal

$$s_{\text{dual}}(t) = s^{(d)}(T,t) + s^{(u)}(T, t - T - T_e) \tag{14}$$

where $s^{(d)}(T,t) = s_{\text{HFM}}(f_h, f_l, T, t)$ and $s^{(u)}(T,t) = s_{\text{HFM}}(f_l, f_h, T, t)$ are the HFM signals with the same frequency band and the opposite sweep directions. Transform the received Doppler scaled signal $x(t) = A \cdot s_{\text{dual}}(k(t-\tau))$ into frequency domain, and calculate the following statistics in the frequency range $(f_l, f_h)$

$$U(f) = f^4 |X(f)|^2 (S(f))^2 \tag{15}$$

where $S(f)$ is the spectrum of $s^{(d)}(T,t)$. Then, $U(f)$ contains a single-frequency complex exponential signal with period $\Delta\tau = \frac{1}{k}(T + T_e) + 2\varepsilon(k)$. By taking the Fourier inverse transform, we obtain the time-domain signal

$$u(t) = \mathcal{F}^{-1}[U(f)] = A^2 C^3 \left\{ \begin{array}{c} \frac{1}{4\pi j} \left[ \begin{array}{c} 2\sqrt{2}\exp\left(j\eta(2)\right) \cdot \frac{\mathrm{d}}{\mathrm{d}t} s^{(d)}(2T,t) + \\ \exp\left(j(\eta(4) - 2\vartheta(k))\right) \cdot \frac{\mathrm{d}}{\mathrm{d}t} s^{(d)}(4T, t + \Delta\tau) \end{array} \right] \\ + C\delta(t - \Delta\tau) \cdot \exp\left(j2\vartheta(k)\right) \end{array} \right\} \tag{16}$$

where $\delta(t)$ is the impulse function, $C = C(T)$ and $\vartheta(k)$ are the parameters in the HFM signal mentioned in Sects 2.1 and 2.2, and the frequency modulation coefficient $M$ is taken as the absolute value. $u(t)$ has a peak at $t = \Delta\tau$ which can be used to derive the Doppler scaling factor estimate. In Eq. (16), we correct the minor error in the previous study [4]. In order to obtain a more accurate estimate, we can take the IDFT on $U(f)$ near $t = \Delta\tau$

$$y(v) = \int_f U(f) \cdot \exp\left(j2\pi f(c_1\alpha(v) + c_2)\right) \mathrm{d}f \tag{17}$$

where $c_1 = T + T_e + 2f_0/M$ and $c_2 = T + T_e$ are constants, and $\alpha(v)$ is the Doppler factor defined as $\alpha(v) = \frac{v}{c}$ for passive situation and $\alpha(v) = \frac{2v}{c-v}$ for active situations. $y(v)$ is called the speed spectrum, and its peak $\hat{v} = \arg\max_v |y(v)|$ gives the estimation of the target speed. The estimation of speed can be obtained by taking the maximum value of $y(v)$ within the possible speed range, and $c_1$, $c_2$ and $\alpha(v)$ can all be preset. The analytical results of underwater communication experimental data have verified the effectiveness of this method [4].

A noteworthy problem is the relationship between the main lobe width of the speed spectrum $y(v)$ and the waveform parameters. Since $U(f)$ does not extend infinitely, the impulse function contained in the speed spectrum $y(v)$ is a sampling function indeed. According to the characteristics of the Fourier transform of the truncated signal, the main lobe width of $y(v)$ can be determined by

$$w_v = \frac{c\left(4f_0^2 - M^2T^2\right)}{2MTf_0^2\left(T + T_e + 2f_0/M\right)} \tag{18}$$

where the main lobe width is defined as the gap between the two zero points of the sampling function. Equation (18) is the result for passive situations, while the main lobe width is about half of (18) for active situations. The increase in the bandwidth/the pulse width can both lead to a thinner main lobe. See Sect. 4.1 for numerical simulation results.

### 3.2 Performance in multipath channel

In underwater applications, the performance of communication system or active sonar is seriously affected by multipath effects. The received signal usually appears as multiple or distributed highlights. The experimental results of the CPM method [7] and the speed spectrum method [4] have shown the effectiveness of dual-HFM-based methods in the multipath channel, but theoretical analysis has not been presented. Next, we will analyze the influence of the multipath channel on the Doppler estimation performance through speed spectrum scanning.

The impact of the multi-path channel is that one received signal frame could consist of multiple dual-HFM signals. They arrive almost simultaneously and cannot be separated on the timeline. Figure 2 sketches the two kinds of multi-path effects. When the multiple sound rays are with different transmit angles, as shown in Fig. 2a, the multiple signals will be separable in the timeline because the sound ranges are different. These multiple signals will appear as they come from different range and with different moving speed, just like multiple objects. The single-frame processing will not be affected in this situation. When the multiple sound rays are with very close transmit angles, as shown in Fig. 2b, the sound ranges will be almost the same and the multiple signals will be included in the same frame. As the transmit angle is close, they are almost related to the same Doppler speed. The impulse response of the channel can be either multiple impulses or a distributed signal. We will next analyze whether this effect will impact the speed spectrum estimation. Figure 2 is an example sketch of sound ray structure, and other sound ray structures can also lead to similar effects.

Firstly, we consider the case of two paths. Let the multipath received signal be the superposition of two signals

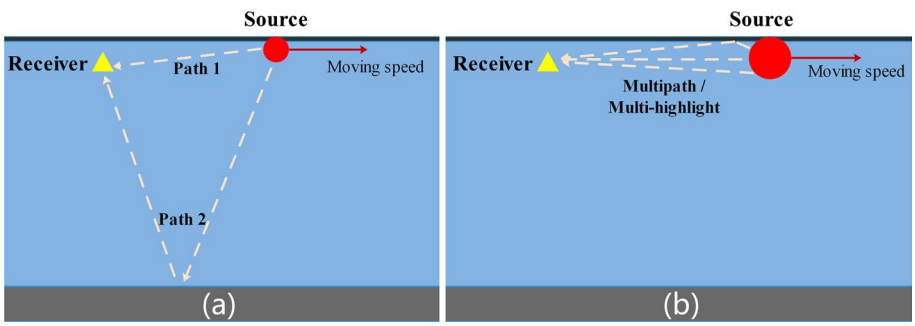


**Fig. 2** Diagrams of the underwater multipath channel: **a** Multipath signals with different transmit angles; **b** multipath signals with close transmit angles

$$x_{\mathrm{MP}}(t) = A_1 x_0(t) + A_2 x_0(t-\mu) \tag{19}$$

with arrival time difference $\mu$, where $x_0(t)$ is the normalized received signal for the single path (i.e., $x(t)$ with $A = 1$ in Sect. 3.1). Then, the spectrum of $x_{\mathrm{MP}}(t)$ is $X_{\mathrm{MP}}(f) = X_0(f) \cdot \left(A_1 + A_2 \cdot \exp\left(-j2\pi f\mu\right)\right)$, and $U_{\mathrm{MP}}(f) = U_0(f) \cdot \left(A_1^2 + A_2^2 + 2A_1A_2\cos\left(j2\pi f\mu\right)\right)$. Therefore, the Fourier inverse transform of $U(t)$ is

$$u_{\mathrm{MP}}(t) = \left(A_1^2 + A_2^2\right)u_0(t) + A_1A_2[u_0(t-\mu) + u_0(t+\mu)] \tag{20}$$

where $X_0(f)$, $U_0(f)$ and $u_0(t)$ are all derived from the normalized $x_0(t)$. It can be seen that $u_{\mathrm{MP}}(t)$ will be composed of three peaks when the received signal is composed of signals from two paths,

$$u_{\mathrm{MP}}(t) \approx C^4 \exp\left(j2\pi\vartheta(k)\right) \cdot \left[\left(A_1^2 + A_2^2\right)\delta(t-\Delta\tau) + A_1A_2\delta((t-\Delta\tau+\mu) + \delta(t-\Delta\tau+\mu))\right] \tag{21}$$

The main peak is still located at $t = \Delta\tau$ corresponding to the Doppler scaling factor $k$, and the amplitude is $\left(A_1^2 + A_2^2\right)$. The intensity of the symmetrical pseudo-peaks is $A_1A_2$. Similarly, for the received signal composed of multiple paths, we have

$$u_{\mathrm{MP}}(t) = \sum_n A_n^2 u_0(t) + \sum_{m\neq n} A_m A_n [u_0(t-(t_m-t_n)) + u_0(t+(t_m-t_n))] \tag{22}$$

The intensity of the main peak is $\sum_i A_i^2$, and the surrounding cross-terms have intensity $A_mA_n$. The peak of the speed spectrum is still located at the actual value of $k$; therefore, we can conclude that the estimation is not biased, despite the decrease in sharpness of the peak.

## 4 Result and discussion

In this section, the performance of the proposed method at different conditions will be illustrated by numerical simulations and experimental tests.

### 4.1 Single point target for different durations

Figure 3 shows the simulation results of the passive speed spectrum with different dual-HFM signal parameters. In Fig. 3a, the sweep range of the signal is $f_l = 2$ kHz,

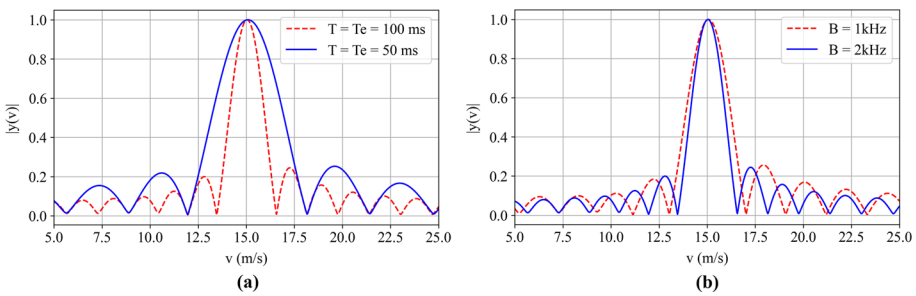


**Fig. 3** The speed spectrum results for different transmit waveform parameters: **a** different pulse width; **b** different bandwidth

$f_h = 4$ kHz, the speed of the source is $v = 15$ m/s, and the speed of sound is 1500 m/s. The curves show the results of the speed spectrum (without noise) for $T = T_e = 50$ ms and $T = T_e = 100$ ms, respectively. In Fig. 3b, the signal duration $T = T_e = 100$ ms and the speed of the source/the sound are the same as the previous. The curves show the results of the speed spectrum (without noise) for the sweep range of the signal are ($f_l = 2$ kHz, $f_h = 4$ kHz) and ($f_l = 2.5$ kHz, $f_h = 3.5$ kHz), respectively. The larger pulse width/bandwidth will lead to a thinner main lobe as is introduced in Eq. (18). A further comparison between the simulation result and the experimental data will be presented in the next section to verify the correctness of the theoretical result.

The concern about the main lobe width lies in situations with interfering signals, such as estimating the Doppler of moving targets in a zero Doppler or noisy background or distinguishing two targets of different speeds. In these cases, we might need to adjust the transmission parameters to obtain a sharper peak.

### 4.2 Single target with multiple paths

In this subsection, two situations of multi-path effect are considered, including a point target with two paths and a distributed target. Figure 4 demonstrates the speed spectrum simulation result for the impulse response of two scenarios, respectively. The transmitted waveform parameter is $f_l = 2$ kHz, $f_h = 4$ kHz and $T = T_e = 100$ ms, the actual speed of the source is $v = 15$ m/s, and the speed of sound is 1500 m/s. In Fig. 4a, the pseudo-peaks in Eq. (21) appear on both sides of the main peak; in Fig. 4b, the superposition of a large number of pseudo-peaks in Eq. (22) leads to the broadening of the

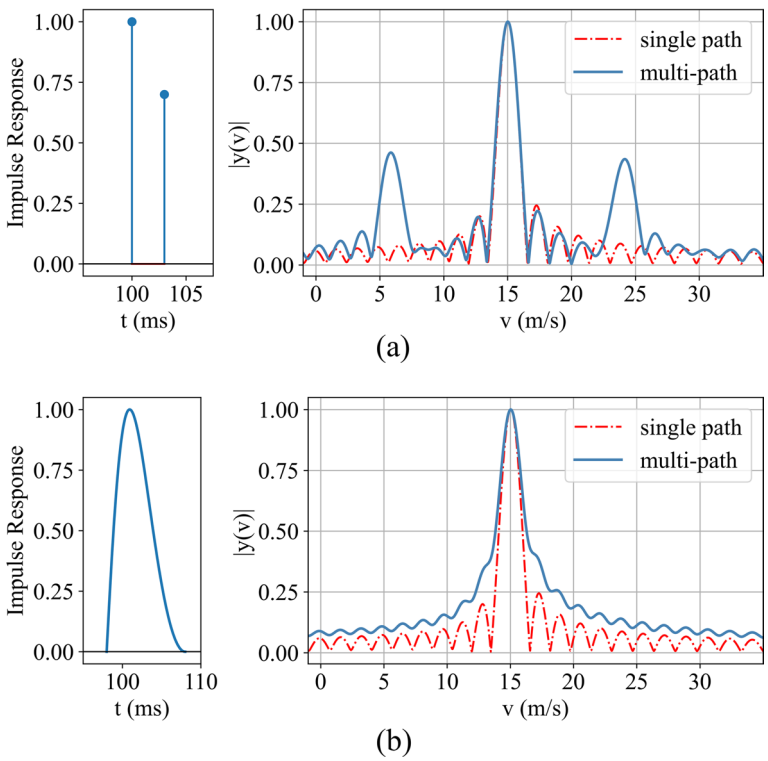


**Fig. 4** Speed spectrum for multipath signal: **a** two-path; **b** distributed

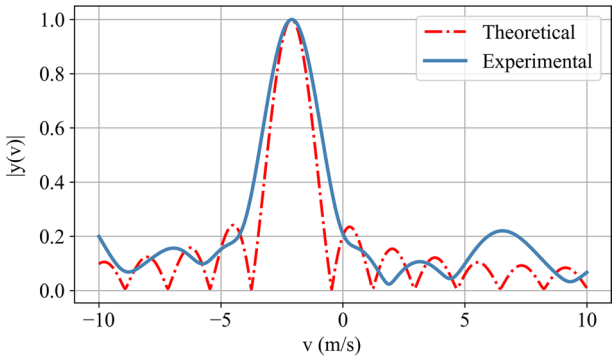


**Fig. 5** Speed spectrum from experimental data, compared with the ideal theoretical result

speed spectrum main lobe and makes the side lobe smoother. Since the peak of the speed spectrum does not shift when it comes to a multipath channel, we can conclude that the method is effective in the underwater environment. In practical application, the main lobe width of the speed spectrum is determined jointly by Eq. (18) and the target/channel distribution characteristics, and the background intensity of the speed spectrum is determined by the side lobe, pseudo-peaks and the noise. In Fig. 5, we compare the speed spectrum between the theoretical result (without noise and multipath effect) and the experimental result [4]. It can be seen that the experimental width of the speed spectrum peak matches the ideal theoretical result, although there is a little spread which is caused by complex factors like velocity spread (acceleration) and multipath distribution effect. This result can further prove that the waveform parameters are the principal determinants of the speed spectrum main lobe width, and the environmental factors including the distributed/multipath channel and the acceleration will make the main lobe spread a little.

## 5 Conclusion

In this paper, we derive and analyze the performance of the speed spectrum estimation method based on the dual-HFM waveform comprehensively. Firstly, we analyze the spectral properties of the HFM signal from the perspective of an ideal DI signal. The derivation could provide insights for better understanding and utilization of the spectrum of the HFM waveform. The speed spectrum method is derived subsequently, and the performance analyses are presented, including the main lobe width and the robustness in the underwater environment. With the theoretical derivation and the comparison between the numerical simulation results and the experimental result, we confirm that this method is effective in a multipath propagation environment, which provides a theoretical explanation for the success in underwater experiments in the previous literature.

**Abbreviations**

| | |
|---|---|
| HFM | Hyperbolic-Frequency-Modulated |
| UMD-HFM | Up-mute-down Hyperbolic-Frequency-Modulated |
| dual-HFM | Dual-Hyperbolic-Frequency-Modulated |
| UWA | The underwater acoustic |
| DI | Doppler invariant |
| CPM | Correlation peak matching |
| DOA | Direction of arrival |

**Acknowledgements**
The authors would like to express their gratitude to the Frontier Exploration Project Independently Deployed by Institute of Acoustics, Chinese Academy of Sciences, QYTS202013

**Author contributions**
RW put forward the original idea of the paper. XM and XL contributed to the validation, review, editing and supervision. RW and YF finished the original draft and the revisions. All authors read and approved the final manuscript.

**Funding**
The research was supported by the Frontier Exploration Project Independently Deployed by Institute of Acoustics, Chinese Academy of Sciences, QYTS202013

**Availability of data and materials**
All data generated or analyzed during this study are included in this paper

## Declarations

**Ethics approval and consent to participate**
All procedures performed in this paper were in accordance with the ethical standards of research community

**Consent for publication**
Not applicable

**Competing interests**
The authors declare that they have no competing interests.

Received: 11 August 2022 Accepted: 16 December 2022
Published online: 28 December 2022

**References**

1. M. Stojanovic, J.A. Catipovic, J.G. Proakis, Phase-coherent digital communications for underwater acoustic channels. IEEE J. Ocean. Eng. **19**(1), 100–111 (1994)
2. B.S. Sharif, J. Neasham, O.R. Hinton, A.E. Adams, A computationally efficient doppler compensation system for underwater acoustic communications. IEEE J. Ocean. Eng. **25**(1), 52–61 (2000)
3. M. Xin, W. Li, X. Wang, Y. Zhang, L. Xu, Preamble design with hfms for underwater acoustic communications, in *2018 OCEANS: MTS/IEEE Kobe Techno-Oceans* (2018), pp. 1–5
4. R. Wei, X. Ma, S. Zhao, S. Yan, Doppler estimation based on dual-hfm signal and speed spectrum scanning. IEEE Signal Process. Lett. **27**, 1740–1744 (2020)
5. K. Wang, S. Chen, C. Liu, Y. Liu, Y. Xu, Doppler estimation and timing synchronization of underwater acoustic communication based on hyperbolic frequency modulation signal, in *2015 IEEE 12th International Conference on Networking, Sensing and Control* (2015), pp. 75–80
6. X. Zhang, F. Kong, H. Feng, Frequency offset estimation and synchronization of underwater acoustic communication with hyperbolic frequency modulation signal. Tech. Acoust. **29**(2), 210–213 (2010)
7. S. Zhao, S. Yan, L. Xu, Doppler estimation based on hfm signal for underwater acoustic time-varying multipath channel, in *2019 IEEE International Conference on Signal Processing, Communications and Computing (ICSPCC)* (2019), pp. 1–6
8. A.W. Rihaczek, Doppler-tolerant signal waveforms. Proc. IEEE **54**(6), 849–857 (1966)
9. J.J. Kroszczynski, Pulse compression by means of linear-period modulation. Proc. IEEE **57**(7), 1260–1266 (1969)
10. E. Fowle, The design of fm pulse compression signals. IEEE Trans. Inf. Theory **10**(1), 61–67 (1964)

## Publisher's Note